FULL PAPER *Anatomy*

Availability of NMR Microscopic Observation of Mouse Embryo Disorder: Examination in Malformations Induced by Maternal Administration of Retinoic Acid

Miki SUGIMOTO[1)], Noboru MANABE[1)]*, Maki MORITA[1)], Takako TANAKA[1)], Reika OKAMOTO[1)], Satoshi IMANISHI[1)] and Hajime MIYAMOTO[1)]

[1)]*Unit of Anatomy and Cell Biology, Department of Animal Sciences, Kyoto University, Kyoto 606–8502, Japan*

(Received 3 December 2001/Accepted 6 February 2002)

ABSTRACT. Nuclear magnetic resonance (NMR) microscopy is a magnetic resonance imaging method with enhanced spatial resolution due to the use of a high static magnetic field and high magnetic field gradients. It is considered to be a useful tool for non-invasive and continuous investigation of tissue and organs at the histological level. In this study, we applied NMR microscopy to assessment of morphology in mouse embryos using a developmental disorder model induced by retinoic acid administration. Pregnant mice were given 50 mg/kg *all-trans* retinoic acid at 8.5 dpc. Embryos were collected at several time points after treatment and examined by NMR microscopy after fixation. Two-dimensional and three-dimensional spin echo sequences were used. Tissue contrast on two-dimensional images changed according to length of repetition time and echo time, and also to developmental stage of embryos. Two-dimensional and three-dimensional images nondestructively demonstrated defects in development of the skeleton and soft tissue, e.g. hypoplasia of vertebrae in the lumbar and tail regions and dysplasia of the spinal cord, in embryos exposed to retinoic acid. These morphological abnormalities were confirmed by conventional assessment after imaging. Although further improvements are required, NMR microscopy will provide a new approach for multi-parameter assessment of embryonic development under physiological and pathological conditions.
KEY WORDS: magnetic resonance imaging, mouse, NMR microscopy, retinoic acid.

J. Vet. Med. Sci. 64(5): 427–433, 2002

Magnetic resonance imaging (MRI) is useful for non-invasive and continuous investigation of objects. Conventional proton (^{1}H) MRI is widely used in the clinical field, especially for detection of disorders in soft tissue that cannot be detected by x-ray computed tomography. Nuclear magnetic resonance (NMR) microscopy is an MRI method with enhanced spatial resolution due to the use of a strong static magnetic field and high magnetic field gradients. In NMR microscopy, spatial resolution is enhanced to sub-millimeter orders [4, 12], while that in traditional MRI is of the order of 1 mm. Using this technique, non-invasive and multi-dimensional observation of small specimens can be performed at a level similar to low power light microscopy. This level of resolution is necessary for investigation of embryo morphology in small animals such as mice, as dimensions in such objects are less than one tenth of those in the clinical field.

In this study, we examined mouse embryos with normal morphology and with malformations induced by retinoic acid administration by NMR microscopy. Retinoic acid is an active metabolite of vitamin A. Although vitamin A is an essential nutrient for mammals including human and domestic animals, excessive intake of vitamin A and retinoic acid in pregnant mammals induces widespread malformation in developing embryos [1–3, 5, 6, 13, 15–17, 21]. We reported previously that a single-shot maternal administration of retinoic acid caused malformations in murine embryos showing characteristic defects in the skeleton depending on dose and developmental stage of embryos at the time of treatment [14]. In embryos given retinoic acid at 8.5 days post coitum (dpc), malformations in the craniofacial and trunk region were observed. Disappearance or severe hypoplasia of the tail occurred in a high proportion of embryos. Atrophy in the tail region by this treatment was noted as early as 11.5 dpc. Skeletal systems in mouse embryos are conventionally analyzed in whole-body skeletal preparations. Processing of conventional skeletal preparations is, however, rather laborious and time consuming. Furthermore, soft tissue must be removed or damaged during processing and cannot be assessed *in situ*. NMR microscopy will be a useful tool for assessment of skeletal defects allowing the simultaneous examination of other structures.

* CORRESPONDENCE TO: MANABE, N., Unit of Anatomy and Cell Biology, Department of Animal Sciences, Kyoto University, Kyoto 606–8502, Japan.

MATERIALS AND METHODS

Animals: Male and female ICR mice were purchased from a local supplier (Clea Japan, Inc., Tokyo, Japan). They were given a commercial diet and water *ad libitum*. They were kept in a temperature-controlled room (22–26°C) under controlled light conditions: 14 hr light and 10 hr darkness with the middle of light period at 12:00 hr. All animal experiments conformed to the Guide for the Care and Use of Laboratory Animals (Kyoto University Animal Care Committee according to NIH #86–23; revised 1985).

Induction of malformation by retinoic acid and collection of embryos: Mature female ICR mice were mated with males of the same strain overnight, and those with vaginal

plugs on the next day were used for experiments. Noon of the day following mating was considered 0.5 dpc. Induction of malformations by administration of retinoic acid was performed as described previously [14]. *All-trans* retinoic acid (RA; Sigma, MO, U.S.A.) dissolved in dimethyl sulfoxide (DMSO) was injected intraperitoneally into each pregnant mouse (50 mg/kg body weight) at 8.5 dpc. Control mice were given DMSO without retinoic acid. At 11.5, 13.5, 15.5 or 18.5 dpc, the pregnant mice were euthanized and embryos were collected. The embryos were fixed in 20% neutral buffered formalin for a minimum of 1 week. Thereafter, embryos were transferred into 10% neutral buffered formalin.

NMR microscopy: Fixed embryos were embedded in 3% low-melting-point agarose (agarose type VII, Sigma, MO, U.S.A.) [18] contained in sample tubes before examination using an NMR microscope, a 400 MHz wide bore spectrometer equipped with a microimaging attachment (NM-AIM imaging equipment, JEOL, Japan). The sample tube with embryo was set at the center of the detection coil (20 or 10 mm in diameter) in an imaging probe. The imaging probe was inserted in a magnet with a static magnetic field of 9.4 T equipped with coils producing magnetic field gradients (11.75 G/cm in the 20 mm probe and 47 G/cm in the 10 mm probe for X, Y and Z axes). NMR microimages were acquired using two-dimensional Fourier transformation spin echo (2DFT-SE) and three-dimensional Fourier transformation spin echo (3DFT-SE) sequences. Fields of view were 30, 20 or 10 mm for each axis. Sizes of probes and fields of view were selected depending on the size of the specimen. Receiver gain was automatically adjusted before each observation. In 2DFT-SE, three or five sagittal images were acquired using a multislice spin echo sequence. Slices were 1 mm in thickness with a gaussian profile (4,000 Hz in the 20 mm probe and 16,000 Hz in the 10 mm probe, gaussian). Intervals between central observation frequencies of neighboring slices were set to 5,000 Hz in the 20 mm probe and 20,000 Hz in the 10 mm probe to adjust the slice intervals to 1 mm. The data matrix of each slice was 256×256. Images were acquired using different values of repetition time (TR), substituted by pulse delay time because of system settings, and echo time (TE). Combinations of TR/TE in milliseconds were 200/5, 500/5, 1,000/5, 1,000/10, or 1,000/20. Number of excitations was 16, 32 or 64. Parameters for 3DFT-SE were as follows; TR/TE = 200/5, data matrix=$128 \times 128 \times 128$ or $256 \times 256 \times 32$; number of excitations=4 or 8. Image reconstruction and visualization were performed by Fourier transformation on a UNIX workstation (DEC3000, Digital Equipment, MA, U.S.A.) by Fourier transformation using "iws" software (JEOL Ltd., Tokyo, Japan), a customized version of NMR/IMAGE (New Methods Research, NY, U.S.A.), or "stork" software (JEOL Ltd., Tokyo, Japan). NMR microimages were exported as Postscript files and transferred to a Macintosh computer. Processing and three-dimensional reconstruction were performed using Adobe PhotoShop software and the public domain image analysis program NIH Image (developed at U.S. National Institute of Health and available on the Internet at http://rsb.info.nih.gov/nih-image/).

Conventional assessments of embryos: Some embryos were processed for skeletal analysis or for light microscopy after NMR microscopy. For skeletal analysis, whole-body skeletal samples by double staining with alcian blue and alizarin red were prepared and examined. For light microscopic examination, embryos were embedded in paraffin and cut serially at a thickness of 5 μm to make sections corresponding to the NMR microimages. Sections were mounted on glass slides, stained with hematoxylin and eosin, and then examined under a light microscope (BX50, Olympus, Tokyo, Japan).

RESULTS

Typical images of a control 18.5-dpc embryo obtained by 2DFT-SE and the effects of TR and TE on tissue contrast are shown in Fig. 1. Major organs appearing in sagittal sections of embryos could be recognized. Acquisition of images with short TR (500 or 200 msec) enhanced the skeletal system. Strong signals in the skeleton were seen in midsagittal sections located in the snout, base of the skull and the spinal column. High intensity signal areas in the spinal column appeared as regular bands across the longitudinal axis. In

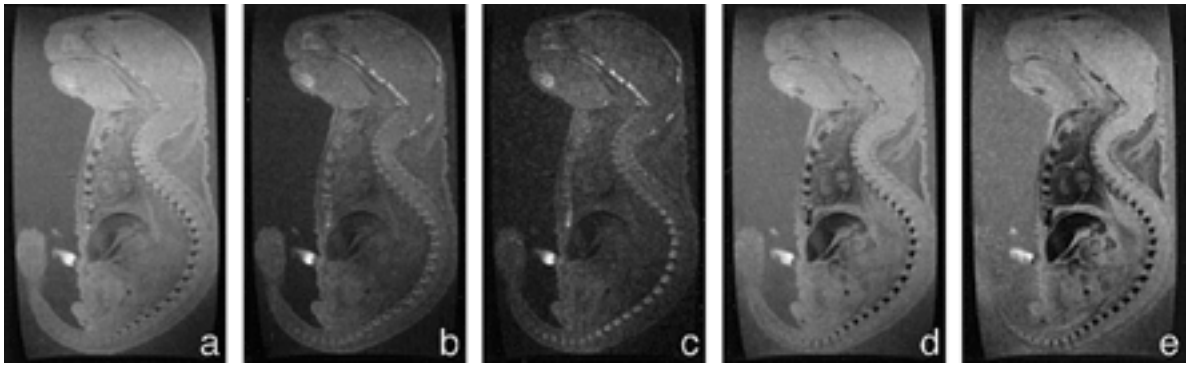

Fig. 1. Effects of TR and TE on 2DTF-SE images showing midsagittal sections of an 18.5 dpc control embryo; a; TR/TE = 1,000/5; b, TR/TE = 500/5; c; TR/TE = 200/5, d; TR/TE = 1,000/10, e; TR/TE = 1,000/20.

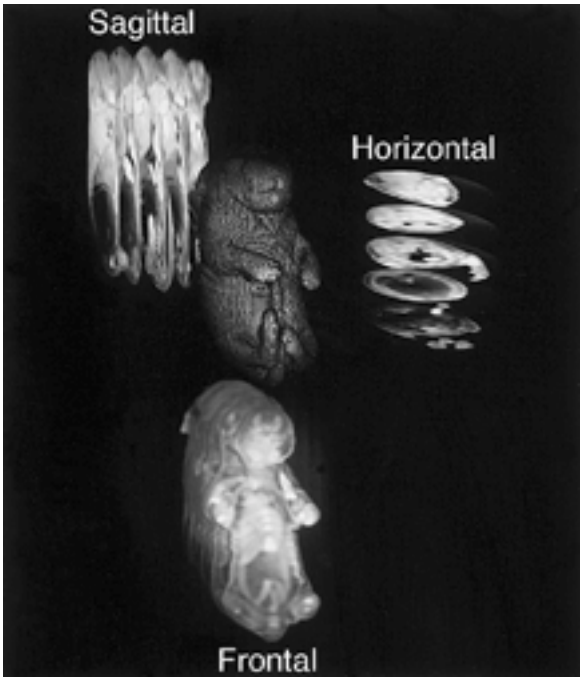

Fig. 2. Surface image and sagittal, frontal and horizontal sections reconstructed from 3DFT-SE data of an 18.5 dpc control embryo. Number of data matrices was 128 for each axis.

images with TE of 10 or 20 msec, connective tissue including bones showed relatively low signal intensity. The hearts and liver also showed weak signals. In 3DFT-SE images, regions with strong signals on orthogonal sections, sliced from three-dimensional data set, were also located mainly in skeletal tissue (Fig. 2). While no notable defects were observed in control 18.5-dpc embryos (Fig. 3a-e), skeletal defects were detected in 2DFT-SE images of 18.5-dpc embryos given RA (Fig. 3f-j). Serious malformations were noted in vertebrae caudad to the lumbar vertebrae. Protrusion of the spinal cord was observed in some cases with defects in vertebrae. Defects in the gastrointestinal tract were also noted. Differences between control embryos (Fig. 4a) and RA-treated embryos (Fig. 4c) were better demonstrated on three-dimensional images reconstructed from 3DFT-SE data. In addition to vertebrae, ilial and ischial hypoplasia were also observed in RA-treated embryos. These malformations in embryos exposed to RA were confirmed macroscopically in skeletal preparations after imaging (Fig. 4b and Fig. 4d).

In 2DFT-SE images of 15.5-dpc embryos, effects of TR and TE on tissue contrast were similar to those in 18.5-dpc embryos (Fig. 5). Regions with strong signals in skeletal tissue on 2DFT-SE images with short TR were less as compared to 18.5-dpc embryos. In 3DFT-SE images, strong signals were observed in regions corresponding to the heart, liver, eyes, and primordial adrenal glands in addition to skeletal tissue (Fig. 6). Malformations in vertebrae and the

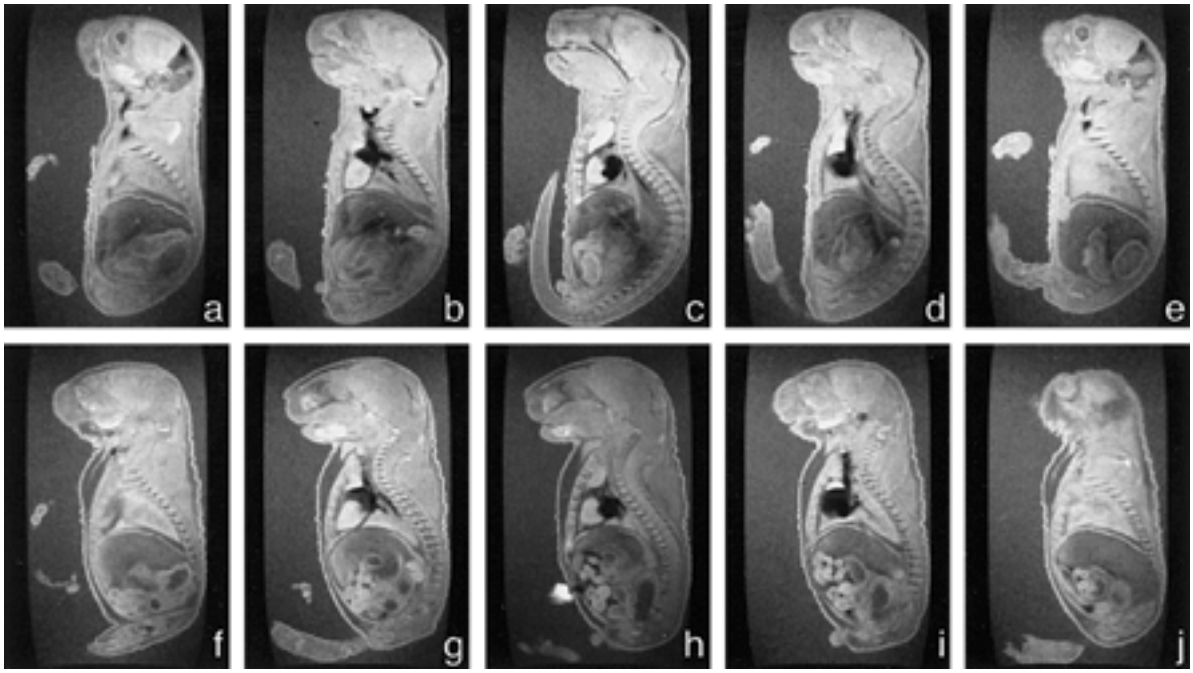

Fig. 3. Multislice 2DFT-SE images of control (a-e) and RA-treated (f-j) embryos at 18.5 dpc. TR/TE=1,000/5. Slice intervals between neighboring images are 1 mm. Images at the center of each row (c and h) are midsagittal sections. Left to right direction in each row corresponds to the left-right axis of embryos. In the RA-treated embryos, the tail was truncated; serious malformations in vertebrae caudad to the lumbar vertebrae, protrusion of the spinal cord, and defects in gastrointestinal tract were observed.

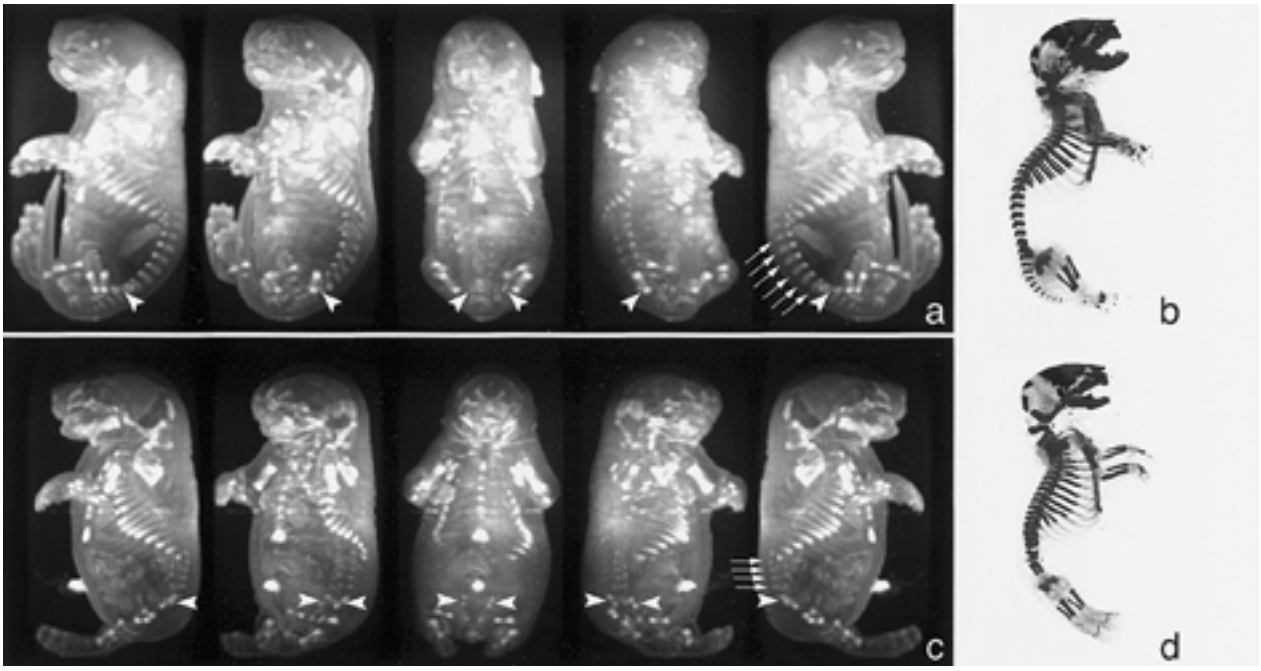

Fig. 4. Rotating projection images reconstructed from 3DFT-SE data of control (a) and RA-treated (c) embryos at 18.5 dpc and lateral views of skeletal preparations of the same embryos after imaging (b and d, respectively). In the RA-treated embryo, caudal vertebrae were lost and only four lumbar vertebrae (arrows in c) were observed, while six (arrows in a) were observed in the control embryo. The ilia (arrowheads in c) and ischia in the RA-treated embryo were hypoplastic as compared with those (arrowheads in a) in the control embryo. Ischia in the RA-treated embryo were positioned in the paramedian position.

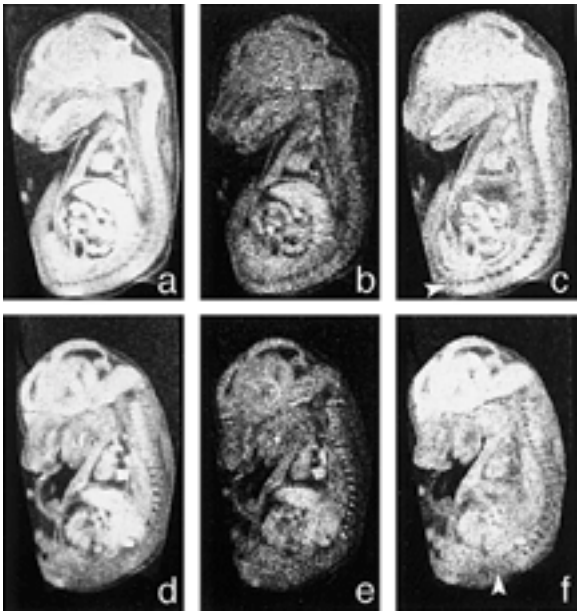

Fig. 5. Effects of TR and TE on 2DTF-SE images showing midsagittal sections of control (a-c) and RA-treated (d-f) embryos at 15.5 dpc; a and d; TR/TE = 1,000/5; b and e, TR/TE = 200/5; c and f; TR/TE = 1,000/20. Effects of TR and TE on tissue contrast were similar to those in 18.5-dpc embryos Malformations in vertebrae and the spinal cord were observed in the RA-treated embryos. Developing vertebrae were observed in the root of the tail in the control embryo (arrowhead in c), however they were not clear in caudal lumber region in the RA-treated embryo (arrowhead in f).

spinal cord were also observed on 2DFT-SE images of 15.5-dpc embryos exposed to RA. These were also noted on histological sections by light microscopy (Fig. 7). Areas with strong signals in images with short TR corresponded to the basis cranii on midsaggital sections. On histological sections, ossification and infiltrating erythrocytes were noted in these regions. Differences in the arrangement of the digestive tract were also noted between embryos exposed to RA and those given vehicle alone. RA-treated embryos showed loose distribution of the digestive tract with hypoplasia in the lower part, although the typical pattern has not yet been defined. In 13.5-dpc (Fig. 8) and 11.5-dpc embryos (Fig. 9), contrast among tissues was decreased compared with embryos in advanced stages of development under the conditions examined. At these stages, atrophy of the tail and precursors of vertebrae in the caudal region were noted in embryos exposed to RA.

DISCUSSION

Many techniques have been developed for assessment of embryo morphology. However, processing for assessment frequently gives rise to irreversible changes in the specimen, decreasing available information. For example, conventional skeletal preparation and light microscopy are both useful but usually mutually exclusive. If a specimen can be examined by multiple techniques, the efficiency of investigation will be enhanced. NMR microscopy used in the

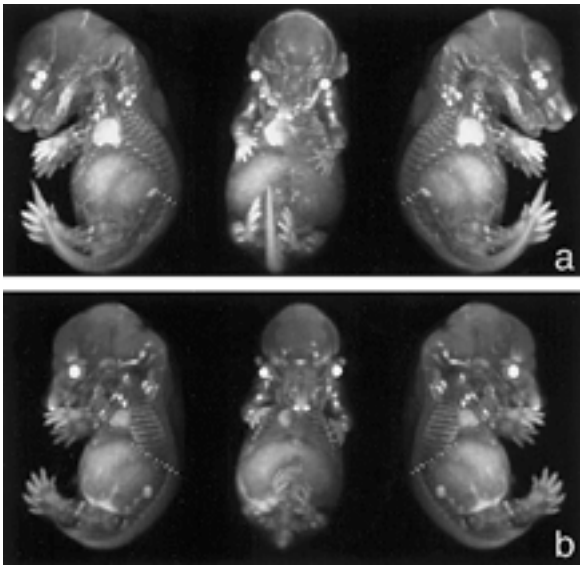

Fig. 6. Rotating projection images reconstructed from 3DFT-SE data of control (a) and RA-treated (b) embryos at 15.5 dpc. Strong signals were observed in regions corresponding to the heart, the liver, eyes, and primordial adrenal glands in addition to skeletal tissue. In the RA-treated embryo, the tail was truncated and caudal vertebrae were aplastic.

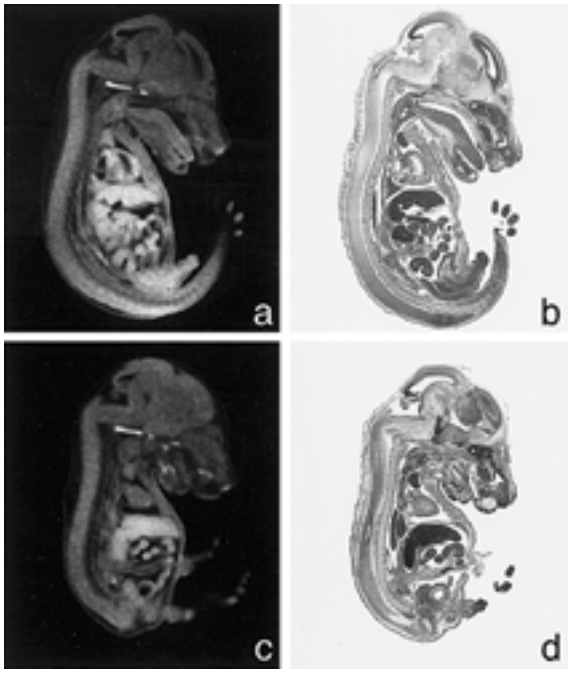

Fig. 7. Midsagittal images of control (a) and RA-treated (c) embryos at 15.5 dpc and corresponding histological sections prepared after imaging (b and d, respectively). TR/TE=500/5. Hypoplasia of lumbar and caudal vertebrae and dysplasia of spinal cord in the RA-treated embryos were observed on both NMR microimages and histological sections.

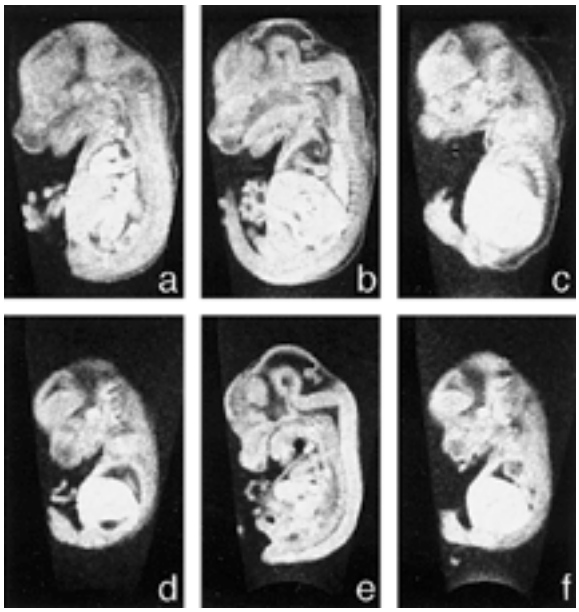

Fig. 8. Multislice 2DFT-SE images of control (a-c) and RA-treated (d-f) embryos at 13.5 dpc. TR/TE=1,000/5. Slice intervals between neighboring images were 1 mm. Images at the center of each row (b and e) are midsagittal sections. Left to right direction in each row corresponds to the left-right axis of embryos. In the RA-treated embryo, structures caudad to the lumbar vertebrae were severely disordered.

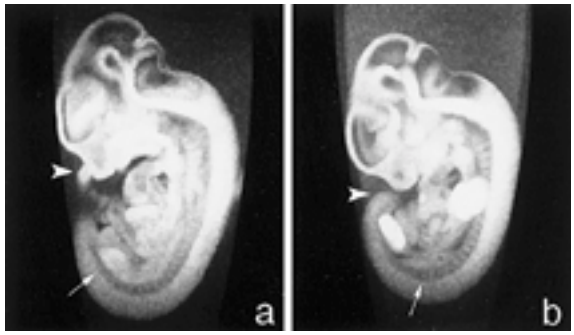

Fig. 9. Superimposed multislice images of control (a) and RA-treated (b) embryos at 11.5 dpc. In the RA-treated embryos, the distal part of the tail (arrowhead in c) was hypoplastic and short compare to that in the control embryo (arrowhead in a). Primitive vertebral structures were formed in the trunk region (arrow in a), while they were also observed in the tail region in the control embryos (arrow in b).

present study could visualize internal structures of embryo specimens without dissection. Using this technique, embryos can be subjected to other kinds of assessments leaving anatomical information as image data. This will be especially useful for specimens with rare or complex traits.

Besides obviation of dissection, NMR microscopic observation can be performed without staining. Contrasts in MRI are produced by differences in the properties of spins within

imaged tissue, such as spin density, spin lattice relaxation time (T1), and spin-spin relaxation time (T2). Differences in T1 and T2 affect changes in signal intensity according to TR and TE, respectively. In the present study, increases in relative signal intensity with short TR were observed in skeletal tissue. Regions with strong signals in short-TR 2DFT-SE images corresponded to ossifying areas in skeleton similarly described by Smith *et al.* [19]. These areas showed strong signals also in 3DFT-SE images acquired with short TR. On 2DFT-SE images with long TE, corresponding areas demonstrated low signal intensity. Mineralized bone in adult animals typically shows weak signals in both T1- and T2-weighted images. However, it has been reported that calcium particles can reduce T1 and T2 relaxation time by a surface relaxation mechanism. Signal intensification in T1-weighted images was observed in some cases in brain calcification [8, 22]. In experimental models, the signal intensity on standard T1-weighted images increases with concentrations of calcium particulate of up to 30% by weight but subsequently decreases due to reduced proton density and reduced T2 [8]. Increases in signal intensity in ossifying skeletal tissue in short-TR images in the present study might have been produced by a similar mechanism. Signal decreases in the liver and heart noted on 2DFT-SE images with long TE would be due to paramagnetic effects of iron derived from hemoglobin. The fetal liver has been reported to show strong signals in T1-weighted images [19], however it was not prominent in our results of 2DFT-SE imaging. Paramagnetic iron particles can decrease both T1 and T2 relaxation times. Signal attenuation due to shortening of T2 in liver tissue was considered to counteracted signal intensification by T1 shortening under the conditions of 2DFT-SE in our system.

In the present study, 2DFT-SE and 3DFT-SE were used. Three-dimensional imaging increases resolution in the direction of slice thickness with the same magnetic field gradient and provides information covering a massive field of view. In the present study, gaussian pulses were used for slice excitation in 2DFT-SE. This improved the blurring of images due to overlapping within the slice thickness, which gave resolution adequate to discern embryo anatomy taking the size of vertebrae as separate structures. However, multislice 2DFT-SE imaging used in this study was not as effective as 3DFT-SE imaging in observation of three-dimensional structure, for example the pelvis. It has been reported that malformation of caudal structures was a typical morphology in embryos exposed to excess RA on 8.5 to 9.5 dpc [14, 16]. Using NMR microscopy, malformation of lumbar and caudal vertebrae, the pelvis, and gastrointestinal tracts were observed. Although vertebral disorder was seen on 2DFT-SE images, hypoplasia of pelvic bones was difficult to observe. The ilia and ischia are oblique against the vertebral column. As multislice images involve gaps between neighboring slices to avoid cross-talk artifacts, structural details may fail to be detected.

Although three-dimensional imaging is useful for assessment of multidimensional structures, it requires a longer time to acquire data of the same matrix number for each axis compared with two-dimensional imaging. Therefore, in 3DFT-SE imaging in the present study, matrix numbers for each axis were reduced compared with those in 2DFT-SE and short TR of 200 msec were used, although these would decrease spatial resolution and signal intensity in most tissue. Consequent imaging time was approximately 15 to 140 min for 2DFT-SE imaging and 7.5 hr for 3DFT-SE imaging with 128^3 matrices. To examine dynamic changes *in vivo*, data acquisition should be performed within a short time frame. Rapid imaging techniques, for example FLASH [7], echo planar imaging [11] and RARE [9], will be useful. Several groups have reported the application of these techniques in NMR microscopy, also in imaging of embryos *in utero* [10, 20]. Introduction of fast imaging techniques will also enable spectroscopic imaging and multinuclear imaging for analysis of metabolic status *in vivo* and provide new approaches for multi-parametric assessment of embryo development under physiological and pathological conditions.

ACKNOWLEDGMENTS. We thank Dr. T. Okuda for development of the malformation induction model by retinoic acid. This work was supported by a Grant-in-Aid for Creative Scientific Research (13GS0008) from the Japan Society for the Promotion of Science, by a Grant-in-Aid for Scientific Research (13027241) from the Ministry of Education, Sports and Culture in Japan, and by a Grant from the Itoh Memorial Foundation.

REFERENCES

1. Abbott, B. D. and Birnbaum, L. S. 1990. Retinoic acid-induced alterations in the expression of growth factors in embryonic mouse palatal shelves. *Teratology* **42**: 597–610.
2. Abbott, B. D., Harris, M. W. and Birnbaum, L. S. 1989. Etiology of retinoic acid-induced cleft palate varies with the embryonic stage. *Teratology* **40**: 533–553.
3. Cusic, A. M. and Dagg, C. P. 1985. Spontaneous and retinoic acid-induced postaxial polydactyly in mice. *Teratology* **31**: 49–59.
4. Eccles, C. D. and Callaghan, P. T. 1986. High-resolution imaging. The NMR microscope. *J. Magn. Reson.* **68**: 393–398.
5. Frenz, D. A., Liu, W., Galinovic-Schwartz, V. and Van De Water, T. R. 1996. Retinoic acid-induced embryopathy of the mouse inner ear. *Teratology* **53**: 292–303.
6. Grant, J. H., Maggio-Price, L., Reutebuch, J. and Cunningham, M. L. 1997. Retinoic acid exposure of the mouse on embryonic day 9 selectively spares derivatives of the frontonasal neural crest. *J. Craniofac. Genet. Dev. Biol.* **17**: 1–8.
7. Haase, A., Frahn, J., Matthaei, D., Hanicke, W. and Merboldt, K.-D. 1986. FLASH imaging. Rapid NMR imaging using low flip-angle pulses. *J. Magn. Reson.* **67**: 258–266.
8. Henkelman, R. M., Watts, J. F. and Kucharczyk, W. 1991. High signal intensity in MR images of calcified brain tissue. *Radiology* **179**: 199–206.
9. Henning, J., Nauerth, A. and Friedburg, H. 1986. RARE imaging: a fast imaging method for clinical MR. *Magn. Reson. Med.* **3**: 823–833.
10. Hogers, B., Gross, D., Lehmann, V., Zick, K., De Groot, H. J.,

Gittenberger-De Groot, A. C. and Poelmann, R. E. 2000. Magnetic resonance microscopy of mouse embryos in utero. *Anat. Rec*. **260**: 373–377.

11. Mansfield, P. 1977. Multi-planar image formation using NMR spin echoes. *J. Phys. C: Solid. State. Phys.* **10**: L55–L58.
12. Neeman, M. and Sillerud, L. O. 1994. NMR microscopy. pp. 101–118. *In*: NMR in physiology and biomedicine (Gillies, R.J. ed.), Academic Press, San Diego.
13. Newall, D. R. and Edwards, J. R. 1981. The effect of vitamin A on fusion of mouse palates. I. Retinyl palmitate and retinoic acid *in vivo*. *Teratology* **23**: 115–124.
14. Okuda, T., Takakuwa, H., Mikami, M., Miyamoto, H. and Manabe, N. 1997. Retinoic acid induces malformations related to cell death in the developing mouse embryo. *J. Reprod. Dev.* **43**: 59–64.
15. Ozeki, H., Shirai, S., Ikeda, K. and Ogura, Y. 1999. Critical period for retinoic acid-induced developmental abnormalities of the vitreous in mouse fetuses. *Exp. Eye Res.* **68**: 223–228.
16. Padmanabhan, R. 1998. Retinoic acid-induced caudal regression syndrome in the mouse fetus. *Reprod. Toxicol.* **12**: 139–151.
17. Padmanabhan, R. and Ahmed, I. 1997. Retinoic acid-induced asymmetric craniofacial growth and cleft palate in the TO mouse fetus. *Reprod. Toxicol.* **11**: 843–860.
18. Smith, B. R., Johnson, G. A., Groman, E. V. and Linney, E. 1994. Magnetic resonance microscopy of mouse embryos. *Proc Natl Acad Sci U.S.A.* **91**: 3530–3533.
19. Smith, B. R., Linney, E., Huff, D. S. and Johnson, G. A. 1996. Magnetic resonance microscopy of embryos. *Comput. Med. Imaging Graph.* **20**: 483–490.
20. Smith, B. R., Shattuck, M. D., Hedlund, L. W. and Johnson, G. A. 1998. Time-course imaging of rat embryos *in utero* with magnetic resonance microscopy. *Magn. Reson. Med.* **39**: 673–677.
21. Stull, D. L. and Wikler, K. C. 2000. Retinoid-dependent gene expression regulates early morphological events in the development of the murine retina. *J. Comp. Neurol.* **417**: 289–298.
22. Suzuki, S., Nishio, S., Takata, K., Morioka, T. and Fukui, M. 2000. Radiation-induced brain calcification: paradoxical high signal intensity in T1-weighted MR images. *Acta. Neurochir. (Wien)* **142**: 801–804.